Velocity distribution and the effect of wall roughness in granular Poiseuille flow

K. C. Vijayakumar and Meheboob Alam*

Engineering Mechanics Unit, Jawaharlal Nehru Center for Advanced Scientific Research, Jakkur PO, Bangalore 560064, India

(Received 27 October 2006; revised manuscript received 6 February 2007; published 22 May 2007)

From event-driven simulations of a gravity-driven channel flow of inelastic hard disks, we show that the velocity distribution function remains close to a Gaussian for a wide range densities (even when the Knudsen number is of order 1) if the walls are smooth and the particle collisions are nearly elastic. For dense flows, a transition from a Gaussian to a power-law distribution for the high-velocity tails occurs with increasing dissipation in the center of the channel, irrespective of wall roughness. For a rough wall, the near-wall distribution functions are distinctly different from those in the bulk, even in the quasielastic limit.

DOI: 10.1103/PhysRevE.75.051306 PACS number(s): 45.70.Mg, 66.30.−h

Granular materials, collections of macroscopic particles, are important in the chemical and pharmaceutical industries as well as in geophysical contexts (avalanches, sand dunes, etc.). In the rapid flow regime [1], the theory for flowing granular materials is largely based on the dense gas kinetic theory which incorporates the *inelastic* nature of particle collisions. At the heart of such gas- or liquid-state continuum theories lies the concept of coarse graining over distribution functions while making a transition from the particle-level properties to the macroscale fields. Unlike the molecular fluid, for which the Maxwell-Boltzmann (Gaussian or Maxwellian) distribution plays the role of the "equilibrium" distribution function, however, the granular fluid does not possess any equilibrium state [1,2] due to the microscopic dissipation of particle collisions. However, there are nonequilibrium (driven) steady states for various canonical granular flow configurations for which the Gaussian distribution is the leading-order velocity distribution [2] in appropriate limits. A systematic study of distribution functions is, therefore, of interest from the viewpoint of developing constitutive models for granular flows as well as to pinpoint the range of validity of any adopted theory. Another important issue that needs attention is the derivation of continuum boundary conditions for granular flows [3] where it is generally assumed that the distribution function in the near-wall region is the same as that in the bulk, which is unlikely to hold as we shall show here.

In driven granular flows, the deviation of the velocity distribution from a Gaussian has been studied through theory [2,4], simulation [5,6], and experiment [7–9]. In Ref. [5] it was shown that the velocity fluctuations in a vibrated bed of particles follow a Gaussian distribution in the solid phase and a power-law distribution (with an exponent −3) in the fluidized phase. For plane shear flow [2], the velocity distribution function is well fitted by an exponent of a second-order polynomial in the norm of the fluctuating velocities with angle-dependent coefficients. Theoretical works [4] for a randomly heated granular gas, based on the Boltzmann-Enskog equation, have predicted velocity distribution functions of the form $P(v) \sim \exp(-\gamma v^{\alpha})$, with the exponent of high-velocity tails being $\alpha = 3/2$, which also depends on the level of inelastic dissipation. Experiments [7] for a granular gas confined between two vertical plates and driven into a steady state via vertical vibrations have shown that $\alpha \sim 1.55 \pm 0.1$, for a wide range of frequency and amplitude of vibrations. Some recent experiments [8], however, showed that the high-velocity tails cannot be described by a single universal exponent.

In this paper we consider granular Poiseuille flow, which is the gravity-driven flow of granular materials through a two-dimensional channel [10], focusing on the rapid flow regime [1]. The simulated system is a channel of length L along the periodic x direction and bounded by two plane solid walls, parallel to the x direction, with a separation of width W (along the y direction). The granular material, consisting of N identical rigid and smooth disks of equal mass and diameter d, is driven by gravity along the x direction. The interactions that are allowed are instantaneous dissipative collisions between pairs of particles and between a particle and the walls, via an event-driven algorithm [11]. The dissipative nature of particle collisions is characterized by the coefficient of normal restitution, e_n, which is the ratio between the pre- and postcollisional relative velocities of the colliding particles. There is no relative tangential velocity since the particles are assumed to be smooth. The solid walls are modeled as frictional surfaces, and a particle colliding with a wall is analogous to a particle colliding with a particle of infinite mass moving at the velocity of the wall. The frictional properties of the walls are modeled using a single parameter, the *coefficient of tangential restitution* for particle-wall collisions (β_w), which is defined as the fraction of relative tangential momentum transmitted from a particle to the wall during a particle-wall collision. The wall roughness is controlled by choosing a specific value of β_w: while $\beta_w = 1$ corresponds to a fully smooth wall, $\beta_w = 0$ corresponds to a fully rough wall for which the dissipation of energy at walls is maximum and there is no relative tangential slip between the particle surface and the wall upon a wall-particle collision.

Apart from the wall-roughness parameter β_w, the granular Poiseuille flow is governed by three control parameters: the average volume fraction (ν), the coefficient of normal restitution (e_n), and the channel width (W/d). It may be noted that the gravitational acceleration (g) does not appear explic-

*Author to whom correspondence should be addressed. Electronic address: meheboob@jncasr.ac.in

itly as a control parameter since it is used as a reference scale for time ($\sqrt{W/g}$), velocity ($\sqrt{Wg}$), and other mean fields. In the present simulation, we have fixed $N=900$ and $W/d=31$ and varied the channel length (L/W) to change the average volume fraction $\nu=\pi N/4(L/W)(W/d)^2$. (The robustness of reported results was checked by increasing the number of particles by fourfold.) The system is initially allowed to attain a statistically steady state for which the streamwise velocity (U_x), volume fraction (ν), and granular temperature (T) remain invariant in time, but have spatial variations along the wall-normal direction (y). All the statistics presented in this paper are computed "binwise" by dividing the channel into 18 bins along the wall-normal direction, and collecting the data in each bin over about 300 000 collisions per particle after reaching the steady state. An increase in the number of bins to 31 did not alter the results; a few bins are indicated by arrows in Fig. 1(b), with bin=1,18 being located adjacent to the walls and bin=9,10 at the center of the channel. It is to be noted that $u_x=c_x-U_x(t)$ and $u_y=c_y$ are the particle fluctuating velocities in the x and y directions, respectively, over the instantaneous mean velocity; here $U_x(t)$ and $U_x=\langle U_x(t)\rangle$ are the instantaneous mean and time-averaged mean streamwise velocity, respectively.

Figure 1(a) shows the probability distribution function of the fluctuating streamwise velocity (u_x) for dilute-to-dense flows ($0.015\leqslant\nu\leqslant0.56$) in different bins. The wall roughness has been set to $\beta_w=0.9$ for smooth walls, and the restitution coefficient to $e_n=0.99$ for quasielastic particle collisions. (The distribution function of the fluctuating transverse velocity u_y looks similar, and hence is not shown.) The local (binwise) distribution functions on only one side of the channel centerline are presented as the distributions on the other side are the same; however, in some cases, the distributions on both sides are presented when they differ. Note that the horizontal axis in the velocity distribution plots is scaled by $\sigma_i=\sqrt{\langle u_i^2\rangle}$, where the index i denotes the coordinate direction, and the vertical axis has been scaled such that $P(0)=1$. It is remarkable that the velocity distribution function in all bins remains Gaussian for a wide range of densities ($\nu<0.6$). This is a surprising result, especially in the dilute limit, since the Knudsen number [see left inset in Fig. 1(a)], which is the ratio between the mean free path and the channel width, $\mathrm{Kn}=l_f/W$, increases with decreasing ν and becomes of $O(1)$ in the dilute limit, signaling the onset of rarefied flow. Even in this rarefied regime, the velocity distribution function remains Gaussian in granular Poiseuille flow with smooth walls. From the profiles of temperature (T), mean velocity (U_x), and volume fraction (ν) in Fig. 1(b), we observe that the mean-field quantities develop considerable gradients along the y direction with increasing density [and this is more pronounced for U_x; see lower inset in Fig. 1(b)], however, they are almost constant over the width of a bin. The mean-field gradients do not seem to play any role in determining the form of local velocity distribution functions as long as the walls are smooth and the particle collisions are quasielastic.

For a dense flow, $\nu=0.56$, with smooth walls $\beta_w=0.9$, Fig. 2(a) shows the effect of collisional dissipation e_n on the form of the $P(u_x)$ distribution in different bins. The velocity distribution in bin=1 (adjacent to the wall), the upper inset in Fig. 2(a), remains close to Gaussian, irrespective of the value of e_n. The $P(u_x)$ distribution in bin=5 (between the wall and the channel centerline), the lower inset in Fig. 2(a), becomes asymmetric with increasing dissipation, with an enhanced probability of negative velocities (negative skewness). At the center of the channel (bin=9), the high-velocity tails of the distribution function undergo a transition from Gaussian to non-Gaussian (with overpopulated tails) with increasing collisional dissipation, as seen in the main panel of Fig. 2(a). The analog of Fig. 2(a) for the fluctuating transverse velocity u_y is shown in Fig. 2(b). The transition of $P(u_y)$ in the channel centerline is very similar to that seen in $P(u_x)$. The distribution in bin=1 remains Gaussian and is not shown here; instead we include the distribution in bin=14. Note that the $P(u_y)$ distributions in bin=5 and bin=14 are mirror images

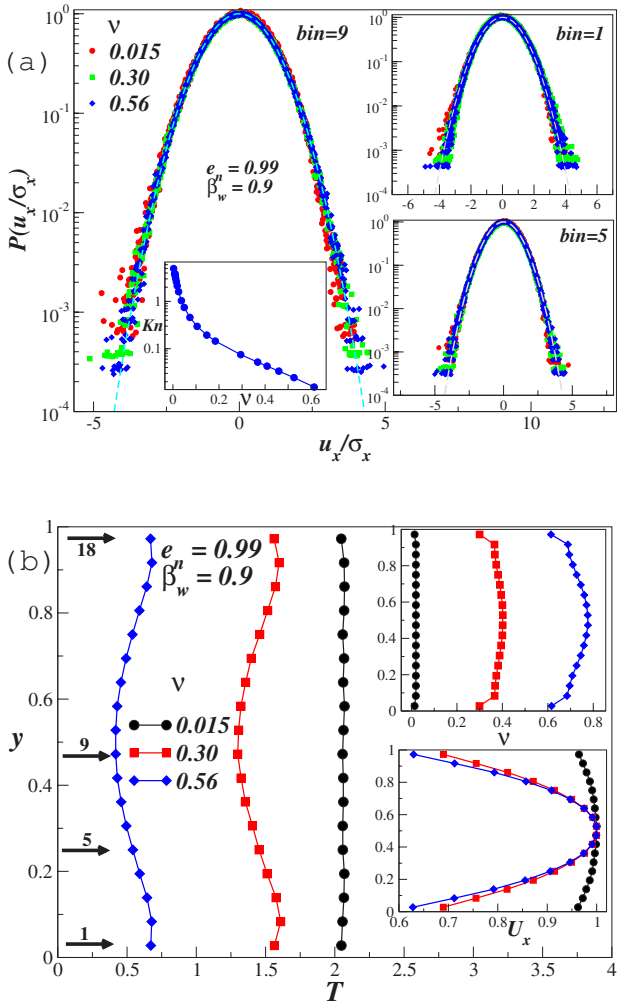

FIG. 1. (Color online) (a) Distribution function of u_x for a range of volume fractions in the quasielastic limit ($e_n=0.99$) for smooth ($\beta_w=0.9$) walls in different bins. The dashed curve indicates a Gaussian. Left inset shows the variation of Knudsen number Kn with volume fraction. (b) Mean velocity (U_x), granular temperature (T), and volume fraction (ν) profiles across the width of the channel for $e_n=0.99$ and $\beta_w=0.9$ at different volume fractions. The arrows near the left ordinate indicate the locations of some bins.

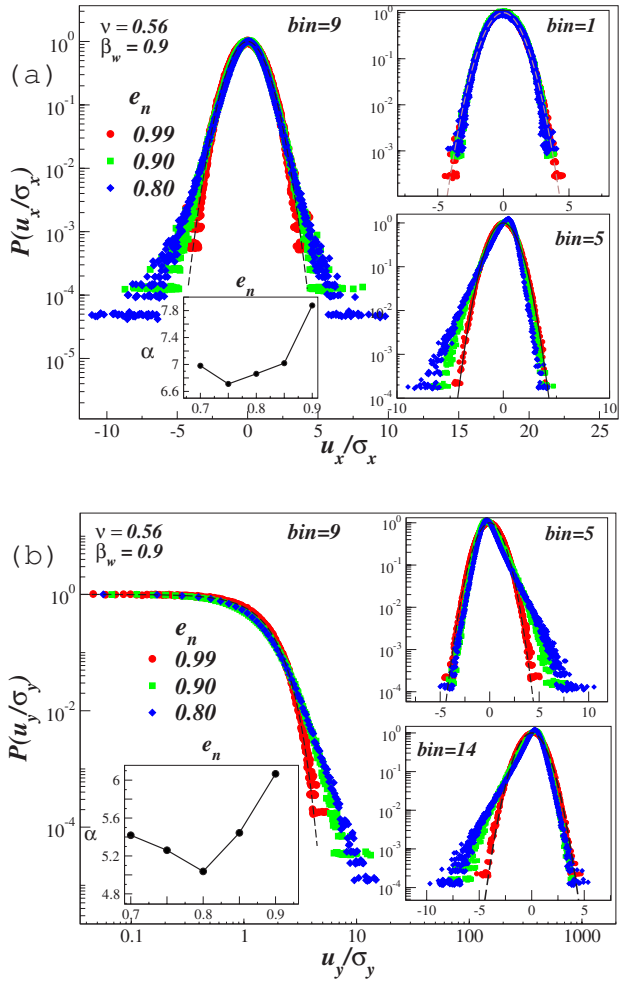

FIG. 2. (Color online) (a) Effect of restitution coefficient, e_n, on $P(u_x)$ at ν=0.56 for smooth walls (β_w=0.9). The velocity distribution in bin=1, upper inset, remains a Gaussian, the distribution in bin=5, lower inset, develops asymmetric tails and the distribution in bin=9 makes a transition from Gaussian to a power-law tails with increasing dissipation. Left Inset: Variation of power-law exponent, α, with e_n. (b) Same as in panel (a) but for $P(u_y)$ in log-log scale to discern the power-law behavior.

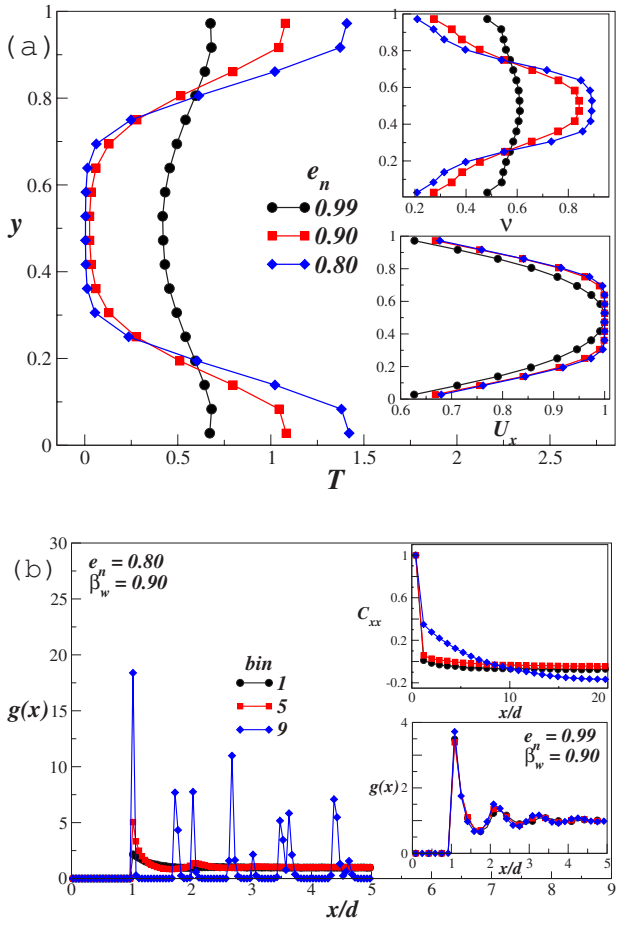

FIG. 3. (Color online) (a) Variations of U_x, T, and ν along y, with parameter values as in Fig. 2. (b) Main panel: Pair correlation function $g(x)$ in different bins at ν=0.56 for e_n=0.8 with smooth walls (β_w=0.9). Upper inset: Streamwise velocity correlation function (C_{xx}) with parameter values as in main panel. Lower inset: $g(x)$ in different bins for e_n=0.99, which shows a liquidlike structure.

since these bins are symmetrically located about the channel centerline. The appearance of asymmetric distribution functions in two shear layers (with increasing dissipation level) could be a consequence of density waves [12] in narrow shear layers. (Within the plug region, however, the local distribution functions are slightly affected by such asymmetries.) This issue is relegated to a future study.

For parameter values as in Fig. 2, the profiles of the mean-field quantities are displayed in Fig. 3(a) which shows the emergence of a plug around the channel centerline (with negligible gradients in U_x, T, and ν) with decreasing e_n, and two shear layers adjacent to two walls with steep gradients in U_x, T, and ν. To pinpoint the role of e_n in the distribution functions, first we study its effect on the pair correlation function and the spatial velocity correlation. The velocity correlation function is defined as follows:

$$C_{ij}(\delta x) = \frac{\langle u_i(x)u_j(x+\delta x)\rangle}{\langle u_i(x)u_i(x)\rangle},$$

where the indices i,j denote the coordinate directions. In the quasielastic limit, the pair correlation function, the lower inset in Fig. 3(b), shows a liquidlike structure in all bins and the velocity correlation is close to zero (not shown). The signatures of plug formation with increasing dissipation show up in the pair correlation function [the main panel of Fig. 3(b)], which indicates a transition from a liquid to a crystal-like structure in bin=9 at e_n=0.8. With increasing density correlation in bin=9, the velocity correlation C_{xx} also becomes strong, as shown in the upper inset of Fig. 3(b). (It is interesting to note that the velocity correlation is negative beyond a certain correlation length $x/d \sim 10$, which is an indicator of circulatory-type motion [13] for the fluctuating velocity field.) At e_n=0.8, the pair correlation function outside the plug region (bin=1,5) shows a gaseous structure, and the C_{xx} correlation is weak or absent [see upper inset in Fig. 3(b)]. Clearly, the enhanced density and velocity correlations around the channel centerline are responsible for the

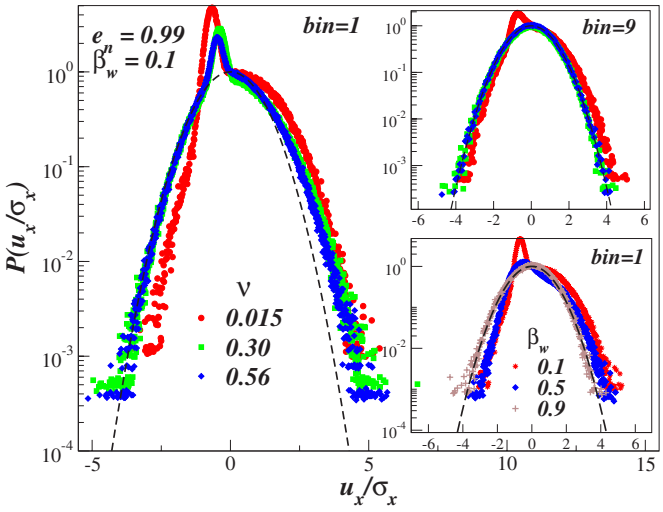

FIG. 4. (Color online) Effect of mean volume fraction on $P(u_x)$ for a rough wall (β_w=0.1) with e_n=0.99 in bin=1. Upper inset: bin=9. Lower inset: Effect of β_w on $P(u_x)$ at ν=0.015 in bin=1.

emergence of non-Gaussian tails with increasing dissipation (Fig. 2).

With reference to dense flows in Fig. 2, the tails of $P(u_i)$ in the plug region can be fitted via a power law of the form $P(u_i) \sim u_i^{-\alpha_i}$, with a single exponent, $\alpha_x \sim 7$ and $\alpha_y \sim 5.5$, for a range of restitution coefficients [see the left insets in Figs. 2(a) and 2(b)]. The near constancy of α_i for $e_n < 0.85$ is due to the fact that the density within the plug saturates to the close-packing limit ($\nu_c \sim 0.9$) for $e_n < 0.85$ and consequently the other hydrodynamic fields also remain invariant there with a further decrease in e_n. This weak variation of α_i with e_n is also implicated in its variation with average density. A similar power-law behavior (with $\alpha \sim 2.9-7.4$) has recently been observed in experiments of gravity-driven channel flow [9]; however, it is difficult to make a direct comparison since the experimental geometry is different (with a sieve at the bottom) and the flow corresponds to the dense quasistatic regime.

The effect of wall roughness on $P(u_x)$ is shown in Fig. 4, for a rough wall β_w=0.1 with quasielastic collisions e_n =0.99. The $P(u_x)$ distribution near the wall (bin=1, main panel) develops a single-peak asymmetric structure at all densities, with its peak being positioned at some negative velocity. Near the centerline (bin=9, upper inset), however, $P(u_x)$ remains asymmetric only at low densities and becomes Gaussian at larger densities. The corresponding $P(u_y)$ distribution (not shown) remains a Gaussian at all densities in the quasielastic limit. For dense flows with rough walls, both $P(u_x)$ and $P(u_y)$ develop power-law tails with decreasing e_n around the channel centerline as in Fig. 2 for smooth walls; the wall roughness did not influence the associated power-law exponents.

Focusing on the dilute regime (ν=0.015), the effect of β_w on $P(u_x)$ in bin=1 is shown in the lower inset of Fig. 4. It is clear that the asymmetry in $P(u_x)$ diminishes with increasing wall smoothness (β_w) and the distribution becomes Gaussian when the walls are smooth (β_w=0.9). This wall-roughness-induced asymmetry in $P(u_x)$ is also reflected in the probability distribution of the instantaneous particle streamwise velocity c_x (not shown), with a single peak in the low-velocity region for bin=1; also, $P(c_x)$ for ν=0.015 approaches a Gaussian with increased wall smoothness. Since the particles lose a significant amount of tangential velocity while colliding with a rough wall in comparison with their collisions with a smooth wall, a peak near the low-velocity region is expected for rough walls. The greater the loss of tangential velocity at walls, the more is the deviation from a Gaussian, and the related asymmetry in Fig. 4 is, therefore, tied to wall roughness. On the whole, in dilute flows the effect of wall roughness is felt on the local distribution functions throughout the channel, whereas for dense flows only the near-wall region is affected.

In conclusion, the local velocity distribution functions in a granular Poiseuille flow (GPF) with smooth walls remain Gaussian for a wide range of densities for nearly elastic collisions ($e_n \to 1$), which, in turn, suggests that the GPF (with smooth walls) could serve as a prototype nonequilibrium steady state to derive constitutive models starting from the Boltzmann-Engkog equation. For dense flows, enhanced density correlations and the related spatial velocity correlations are responsible for the emergence of power-law tails with increasing collisional dissipation around the channel centerline (irrespective of wall roughness) where the flow undergoes a transition from a liquidlike to a crystal-like (plug) structure in the same limit. For a rough wall, the near-wall distribution functions are significantly different from those in the bulk at all densities which calls for a reconsideration of the derivation of granular boundary conditions [3].

[1] L. P. Kadanoff, Rev. Mod. Phys. **71**, 435 (1999); I. Goldhirsch, Annu. Rev. Fluid Mech. **35**, 267 (2003).
[2] N. Sela and I. Goldhirsch, J. Fluid Mech. **361**, 41 (1998); I. Goldhirsch and M. Tan, Phys. Fluids **8**, 1752 (1996).
[3] M. W. Richman, Acta Mech. **75**, 227 (1988); J. T. Jenkins, J. Appl. Mech. **59**, 120 (1992).
[4] T. van Noije and M. Ernst, Granular Matter **1**, 52 (1998); S. Esipov and T. Pöschel, J. Stat. Phys. **86**, 1385 (1997).
[5] Y. Taguchi and H. Takayasu, Europhys. Lett. **30**, 499 (1995); A. Puglisi, V. Loreto, U. M. Marconi, A. Petri, and A. Vulpiani, Phys. Rev. Lett. **81**, 3848 (1998).
[6] R. Cafiero, S. Luding, and H. J. Herrmann, Phys. Rev. Lett. **84**, 6014 (2000); S. J. Moon, J. B. Swift, and H. L. Swinney, Phys. Rev. E **69**, 011301 (2004); J. S. van Zon and F. C. MacKintosh, Phys. Rev. Lett. **93**, 038001 (2004).
[7] F. Rouyer and N. Menon, Phys. Rev. Lett. **85**, 3676 (2000); W. Losert, D. Cooper, J. Delour, A. Kudroli, and J. P. Gollub, Chaos **9**, 682 (1999).
[8] D. L. Blair and A. Kudrolli, Phys. Rev. E **64**, 050301(R) (2001); G. Baxter and J. Olafsen, Nature (London) **425**, 680

(2003).
[9] S. Moka and P. R. Nott, Phys. Rev. Lett. **95**, 068003 (2005); V. Natarajan and M. Hunt, J. Fluid Mech. **304**, 1 (1995).
[10] C. Denniston and H. Li, Phys. Rev. E **59**, 3289 (1999); E. Liss, S. Conway, and B. Glasser, Phys. Fluids **14**, 3309 (2002).
[11] B. Lubachevsky, J. Comput. Phys. **94**, 255 (1991).
[12] J.-C. Tsai, W. Losert, G. A. Voth, and J. P. Gollub, Phys. Rev. E **65**, 011306 (2001); K. C. Vijayakumar and M. Alam (unpublished).
[13] Y. Murayama and M. Sano, J. Phys. Soc. Jpn. **67**, 1826 (1998).